Bioorganic Chemistry 114 (2021) 105080

Contents lists available at ScienceDirect

Bioorganic Chemistry

journal homepage: www.elsevier.com/locate/bioorg

Design, green synthesis, antioxidant activity screening, and evaluation of protective effect on cerebral ischemia reperfusion injury of novel monoenone monocarbonyl curcumin analogs

Wenfei He [a,b,1], Jingsong Wang [b,1], Qiling Jin [b,1], Jiafeng Zhang [b,1], Yugang Liu [c,1], Zewu Jin [b], Hua Wang [c], Linya Hu [b], Lu Zhu [c], Mengya Shen [a], Lili Huang [d], Shengwei Huang [c], Wulan Li [c,*], Qichuan Zhuge [c,*], Jianzhang Wu [a,b,*]

[a] Department of Gynecology and Obstetrics, The Second Affiliated Hospital and Yuying Children's Hospital of Wenzhou Medical University, Wenzhou, Zhejiang 325000, China
[b] Chemical Biology Research Center, School of Pharmaceutical Sciences, Wenzhou Medical University, Wenzhou, Zhejiang 325035, China
[c] The First Affiliated Hospital of Wenzhou Medical University, Wenzhou, China
[d] Department of Pharmacy, Ningbo Medical Centre Lihuili Hospital, Ningbo, Zhejiang 315041, China

ARTICLE INFO

Keywords:
Monoenone monocarbonyl curcumin analogs
Michael acceptor
Toxicity
Antioxidant activity
Cerebral ischemia reperfusion injury
Stroke

ABSTRACT

Antioxidants with high efficacy and low toxicity have the potential to treat cerebral ischemia reperfusion injury (CIRI). Dienone monocarbonyl curcumin analogs (DMCA) capable of overcoming the instability and pharmacokinetic defects of curcumin possess notable antioxidant activity but are found to be significantly toxic. In this study, a novel skeleton of the monoenone monocarbonyl curcumin analogue sAc possessing reduced toxicity and improved stability was designed on the basis of the DMCA skeleton. Moreover, 32 sAc analogs were obtained by applying a green, simple, and economical synthetic method. Multiple sAc analogs with an antioxidant protective effect in PC12 cells were screened using an H_2O_2-induced oxidative stress damage model, and quantitative evaluation of structure–activity relationship (QSAR) model with regression coefficient of $R^2 = 0.918921$ was built through random forest algorithm (RF). Among these compounds, the optimally active compound **sAc15** elicited a potent protective effect on cell growth of PC12 cells by effectively eliminating ROS generation in response to oxidative stress injury by activating the Nrf2/HO-1 antioxidant signaling pathway. In addition, **sAc15** exhibited good protection against CIRI in the mice middle cerebral artery occlusion (MCAO) model. In this paper, we provide a novel class of antioxidants and a potential compound for stroke treatment.

1. Introduction

Stroke, a major cerebrovascular disease worldwide, is associated with high morbidity, disability, and mortality in people aged >40 years [1]. Stroke is divided into two main categories: ischemic and hemorrhagic. Ischemic stroke accounts for ~87% of all strokes [2]. At present, thrombolytic therapy to recover blood reperfusion is considered to be the most efficacious clinical strategy for treating stroke [3,4]. However, reperfusion can also aggravate brain-tissue injury, a process called "cerebral ischemia–reperfusion injury" (CIRI) [5].

Among the various mechanisms underlying CIRI, oxidative stress is a main pathogenic mechanism that occurs at the outset [6–8]. Antioxidants have been widely used to treat CIRI by removing the reactive oxygen species (ROS) generated by oxidative stress through activation of the nuclear factor erythroid 2-related factor 2 (Nrf2) antioxidant signaling pathway. Indeed, this is a reportedly effective therapeutic strategy for CIRI [9,10]. Although intensive studies and even clinical trials have been conducted in this area, very few drugs capable of activating the antioxidant signaling pathway have been authorized for clinical therapy [11]. Therefore, research into powerful and low-toxicity antioxidants for therapy against CIRI is urgently needed.

Currently, leading compounds derived from natural products have

* Corresponding authors at: Chemical Biology Research Center, School of Pharmaceutical Sciences, Wenzhou Medical University, Wenzhou, Zhejiang 325035, China (W. Li, J. Wu).
E-mail addresses: lwlwzmu@163.com (W. Li), qc.zhuge@wmu.edu.cn (Q. Zhuge), wjzwzmu@163.com (J. Wu).
[1] These authors contribute to this work equally.

https://doi.org/10.1016/j.bioorg.2021.105080
Received 13 March 2021; Received in revised form 7 June 2021; Accepted 8 June 2021
Available online 16 June 2021

emerged as biotherapeutic sources for the discovery and development of drugs [12–14]. Curcumin, an active and almost non-toxic small-molecule product extracted from the rhizomes of *Curcuma longa*, exhibits strong antioxidant activity by activating the Kelch-like ECH-associating protein 1/Nrf2-antioxidant response element (Keap1/Nrf2/ARE) antioxidant signaling pathway [15–19]. More than 100 curcumin-related clinical trials have been launched (https://clinicaltrials.gov), but significant progress has not been made. This situation can be explained (at least in part) by the poor stability, low bioavailability, and pharmacokinetic deficiencies caused by an unstable β-diketone moiety in the curcumin skeleton [20–24]. Consequently, much attention has been focused on improving the stability of curcumin while retaining or increasing its biological activities [25–27].

The α,β-unsaturated ketone moiety (a natural Michael acceptor) is a common introduction group in drug molecules [28] and pharmacophore that plays a pivotal role in the antioxidant activity of curcumin [28,29]. Thus, the scaffold of an α,β-unsaturated ketone has always been retained during the structural modification of curcumin [25,30,31]. By removing a single carbonyl group from the unstable β-diketone moiety in the curcumin skeleton, dienone monocarbonyl curcumin analogs (DMCAs) were obtained (Ac in Fig. 1A). This change has greatly improved the stability and pharmacokinetic properties of curcumin while maintaining its original antioxidant activity [32]. However, in subsequent studies, monocarbonyl curcumin analogs showed a certain degree of toxicity [30,33].

In addition, some reports have indicated that the presence of the Michael acceptor in molecules often resulted in distinct toxicity simultaneous with exhibition of antioxidant activity [34]. However, it has been shown in our previous study that chalcones (which are present in various fruits and vegetables) possess a broad range of pharmacological activities and contain a Michael acceptor in the skeleton, but are nearly non-toxic [35]. The reason for this phenomenon may be that the Michael acceptor in the skeleton of chalcones comprises only one double bond, whereas that in DMCAs contains two double bonds. Based on this analysis, it was hypothesized that the toxicity of DMCAs might be reduced by removing an olefinic double bond in the skeleton.

Thus, in the present study, a new scaffold was created by removing an olefinic double bond and a benzene ring from the skeleton of the DMCA (Ac). That is, a novel scaffold of a monoenone monocarbonyl curcumin analog (sAc) was designed (Fig. 1A). A cytotoxicity assay revealed that sAc (10 μM) did not elicit obvious growth inhibition of PC12 cells compared with the significant inhibitory effect of curcumin and the DMCA skeleton Ac. Meanwhile, in a model of H_2O_2-induced oxidative-stress damage, sAc could significantly increase the viability of PC12 cells, whereas curcumin and Ac could not (Fig. 1C, D). In addition, the results of stability determination in phosphate-buffered saline showed that, with the prolongation of time, the OD value of curcumin (Cur) and its skeleton (Cur-S) decreased sharply, and that of the DMCA skeleton Ac also decreased notably, suggesting that they were degraded as a result of structural instability. In contrast, the OD value of sAc showed no variation, indicating its exceptional stability (Fig. 1B). Overall, the new skeleton sAc effectively reduced toxicity, improved stability and, more importantly, greatly enhanced antioxidant protection.

In our study, a series of analogs bearing the novel skeleton sAc were designed and synthesized by applying an environmentally friendly ("green") method [36,37]. In addition, their antioxidant activity and protective effects upon CIRI were evaluated.

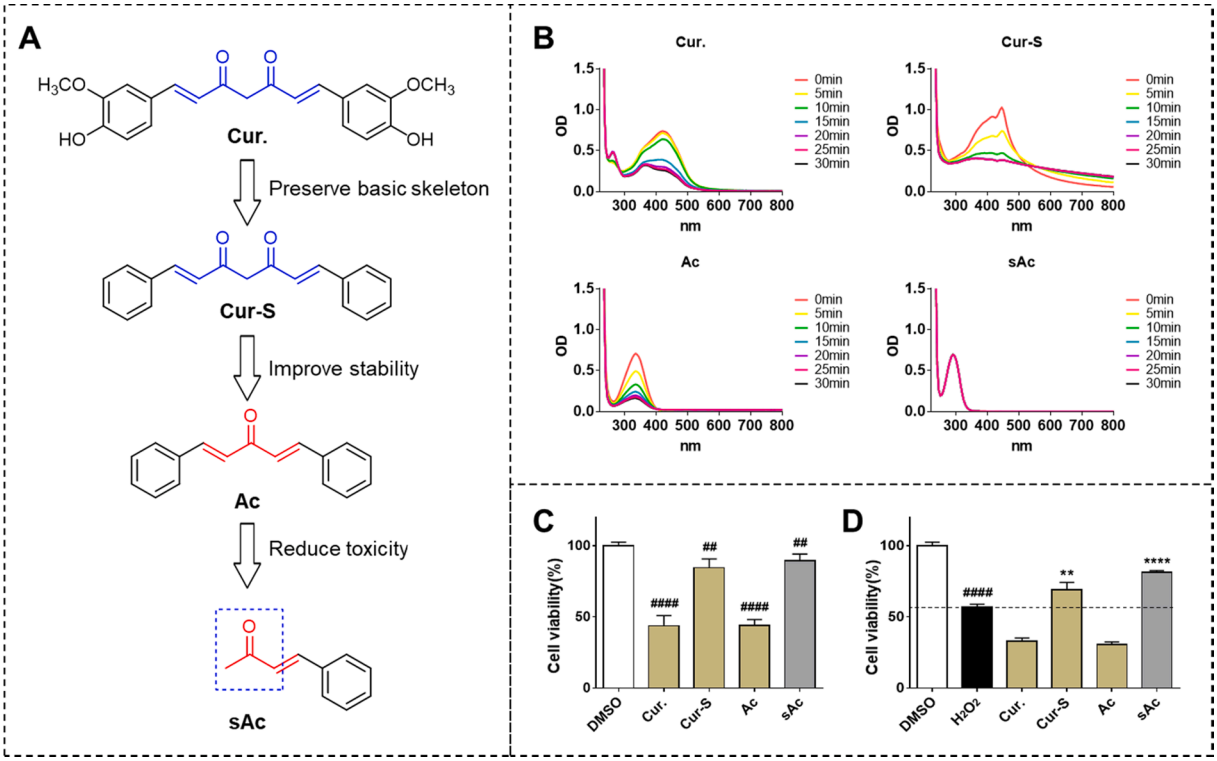

Fig. 1. The design of monoenone monocarbonyl curcumin analogs (A) The design process from the parent compound to the monoenone monocarbonyl curcumin analogs skeleton (B) Structural stability comparison of the curcumin (**Cur.**), curcumin skeleton (**Cur-S**), diketene monocarbonyl curcumin analogs skeleton (**Ac**) and monoenone monocarbonyl curcumin analogs skeleton (**sAc**) (C, D) The cytoprotection and cytotoxicity of curcumin and its different modified skeletons. Cells were incubated with the 10 μM of Cur., Cur-S, Ac and sAc for 42 h (C), and the cytotoxicity of skeletons was determined by the MTT assay. PC12 cells were pre-treated with Cur., Cur-S, Ac and sAc (10 μM) for 18 h and then exposed to H_2O_2 (640 μM) for 24 h (D). The protection of compounds finally determined by the MTT assay and the viability of untreated cells (with 60% DMSO) defined as 100%. Data are expressed as the mean ± SD, n = 3. $^{\#\#\#\#}$ $p < 0.0001$, $^{\#\#}$ $p < 0.01$ vs DMSO, $^{****}p < 0.0001$, $^{**}p$□0.01 vs H_2O_2.

2. Results and discussion

2.1. Green synthesis

We used proline as a catalyst to synthesize the monoketene monocarbonyl curcumin analog sAc, which takes acetone as the bridge ketone (Scheme 1). All compounds (**sAc1–sAc32**) were obtained in reactions of acetone with the appropriate aldehyde at room temperature. All compounds were purified by column chromatography and obtained in high yields (40%–71%) after purification (Table 1). This method compensates for the shortcomings of traditional synthetic methods (e.g., complicated steps, harsh reaction conditions, and low yield), simplifies the reaction steps, improves yields, reduces pollution, and realizes green synthesis.

2.2. Cytotoxicity screening and protective effect of curcumin derivatives on PC12 cells and structure–activity relationship (SAR)

An adrenal pheochromocytoma cell line from rats (PC12) exhibits the general characteristics of neuroendocrine cells and is used widely in neurophysiological and neuropharmacological research [39]. The cytotoxic activity of monoketene monocarbonyl curcumin analogs was first evaluated by analyzing their effects on the growth of PC12 cells, in direct comparison with the parent natural products and tertiary butylhydroquinone (TBHQ), a well-known activator of Nrf2. None of the compounds (**sAc1–sAc32**) displayed significant cytotoxicity to PC12 cells compared with curcumin or piperlongumine (PL) control groups (Fig. 2A). Furthermore, the curcumin derivatives **sAc(1–7)**, **sAc12**, **sAc15**, **sAc(18–20)**, **sAc23**, **sAc25**, **sAc30** and **sAc31** showed even less cytotoxicity than TBHQ.

Uncontrolled ROS production exceeds the clearance capacity of the endogenous defense system. This action causes excessive ROS accumulation and, ultimately, results in secondary oxidative stress and apoptosis in neurons [40]. Hydrogen peroxide (H_2O_2), an important ROS, is often used to induce oxidative damage and apoptosis of neurons *in vitro* [41,42]. Therefore, a model of H_2O_2-induced oxidative damage was used to assess the cytoprotective activity of compounds. Cell viability after oxidative damage was ~55% that of the solvent [dimethyl sulfoxide (DMSO)] group (Fig. 2B). In most groups pre-incubated with compounds, the cell-survival rate improved to 70%–80%. The protective activity of **sAc15** and nineteen other compounds (**sAc(1–5)**, **sAc7**, **sAc9**, **sAc14**, **sAc(16–24)**, **sAc27** and **sAc32**) was even better than that of TBHQ. It should be noted that the cell-survival rates of curcumin and PL groups were lower than that of the H_2O_2 group, which may be related to their own toxicity.

Based on the cell-survival rates of **sAc1-sAc32** (at 10 μM), a structure–activity relationship (SAR) was analyzed. The 3,4-dihydroxy curcumin derivatives (**sAc15**) showed superior protective effects in Fig. 2B and Table 1. With the decrease of the hydroxyl groups on the benzene ring, the antioxidant protection of the analogs [**sAc13** (3-hydroxy), **sAc14** (4-hydroxy)] weakened. Meanwhile, in contrast to the hydroxy, the antioxidant activity of the analogs containing one methoxy group [**sAc2** (2-methoxy) or **sAc4** (4-methoxy)] was stronger than that of the two or more methoxy groups [**sAc6** (2,4-dihydroxy) and **sAc11** (2,4,6-trimethoxy)]. Consequently, dihydroxy and monomethoxy groups can enhance the antioxidant activity, but that of monomethoxy could be not comparable to dihydroxy.

Table 1
The monoenone monocarbonyl curcumin analogs.

Comp.	R in ring	Yields	Comp.	R in ring	Yields
sAc1	H	70%	**sAc17**	3-OCH_3, 4-OH	56%
sAc2	2-OCH_3	66%	**sAc18**	3,5-OCH_3, 4-OH	44%
sAc3	3-OCH_3	68%	**sAc19**	3-CHO	40%
sAc4	4-OCH_3	71%	**sAc20**	3-F	57%
sAc5	2,3-OCH_3	65%	**sAc21**	4-F	60%
sAc6	2,4-OCH_3	67%	**sAc22**	3,4-F	51%
sAc7	2,5-OCH_3	64%	**sAc23**	3,5-F	55%
sAc8	3,4-OCH_3	61%	**sAc24**	3-Cl	56%
sAc9	3,5-OCH_3	67%	**sAc25**	4-Cl	61%
sAc10	2,4,5-OCH_3	59%	**sAc26**	3,5-Cl	57%
sAc11	2,4,6-OCH_3	57%	**sAc27**	4-Br	62%
sAc12	3,4,5-OCH_3	57%	**sAc28**	4-$N(CH_3)_2$	61%
sAc13	3-OH	50%	**sAc29**	4-$N(C_2H_5)_2$	58%
sAc14	4-OH	48%	**sAc30**	4-Piperidinyl	54%
sAc15	3,4-OH	45%	**sAc31**	4-Morpholin	51%
sAc16	3-OH, 4-OCH_3	52%	**sAc32**	/[a]	55%

2.3. Quantitative evaluation of structure–activity relationship (QSAR)

QSAR is widely used in drug development as a means to guide drug design. In recent years, QSAR based on machine learning has been widely used, among which random forest algorithm (RF) is one of the effective machine learning algorithms for building QSAR model [38]. RF is to generate multiple different sub data sets by sampling the total data set, and train a decision tree for each sub data set. After that, the prediction results of each decision tree are combined as the final prediction results. In this study, QSAR model was built through RF based on the corresponding data of cell viability after oxidative damage. As shown in the Fig. 3, the abscissa represents the cell-survival rate, and the ordinate represents the value calculated by the QSAR. Regression coefficient of $R^2 = 0.918921$ with excellent fitting result, and the data distribution of the QSAR with uniform has a certain guidance for the follow-up research. **sAc15** (blue) is noted at the upper right of the Fig. 3.

2.4. *sAc15* inhibited H_2O_2-induced cell damage to PC12 cells

Considering the toxicity of compounds (**sAc1–sAc32**) and their protective effect on PC12 cells, compound **sAc15** was selected as the active compound for further research. Compound **sAc15** contains two phenolic hydroxyl groups, which could directly and indirectly scavenge free radicals through antioxidant pathways, and exert excellent dual antioxidant activities [8]. **sAc15** protected cells damaged by H_2O_2-induced oxidation and promoted colony formation, further confirming the cytoprotective effect of **sAc15**. The damage induced by H_2O_2 severely inhibited the colony formation of PC12 cells (Fig. 4A), but this effect was reversed by **sAc15** at very low concentrations. Indeed, the colony-formation effect of **sAc15** was far superior to that of the positive control drug TBHQ (2.5 μM). In addition, cells with different concentrations of **sAc15** were pre-incubated to evaluate its antioxidant activity *in vitro*. After treatment with **sAc15**, cell-survival rates increased with increasing doses in the range of 0.625–20 μM (Fig. 4B). Thus, the protective effect of **sAc15** clearly exceeded that of TBHQ at 20 μM.

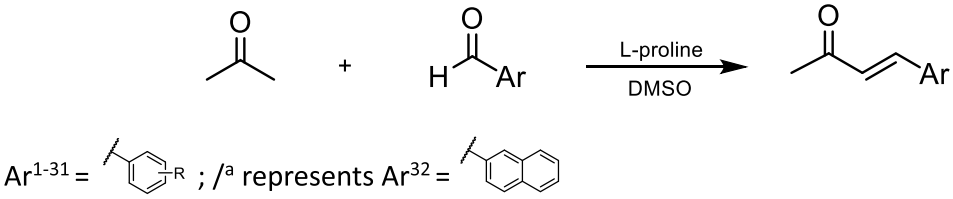

Scheme 1. Synthesis and structures of monoenone monocarbonyl curcumin analogs. Synthetic conditions: (I) L-proline, DMSO, room temperature.

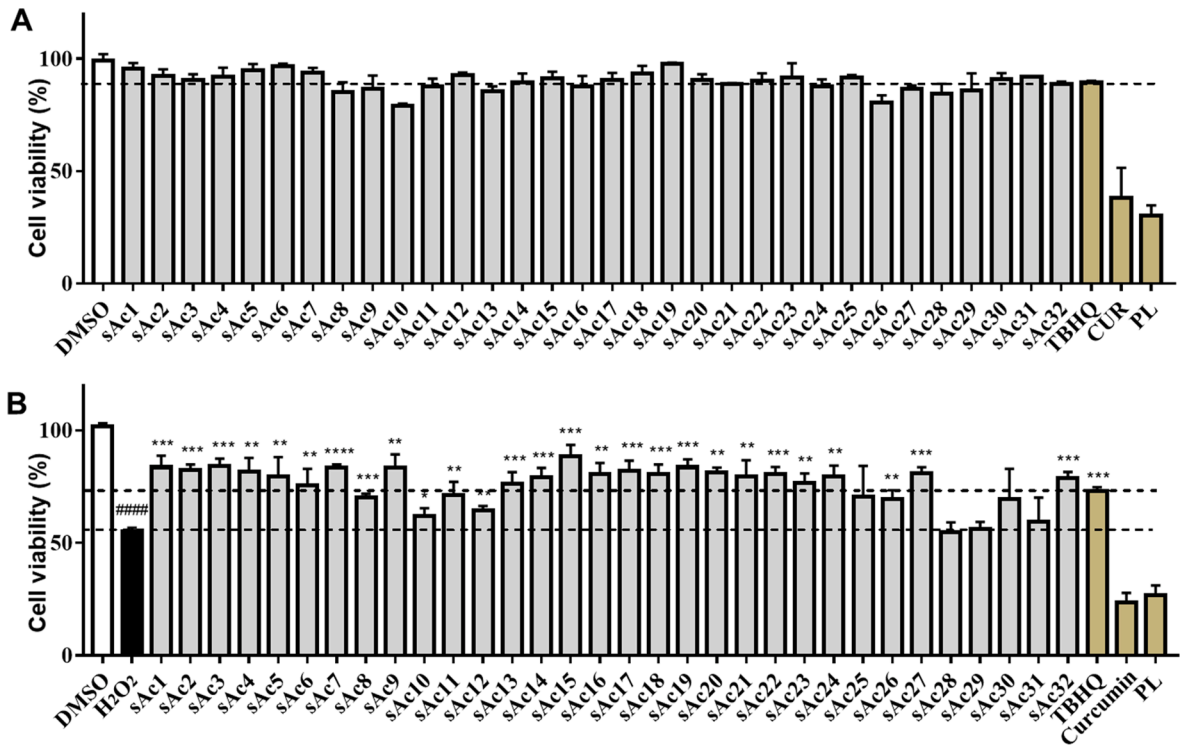

Fig. 2. Compounds' cytotoxicity screening on PC12 cells (A) and its cytoprotection on PC12 cells in H_2O_2 damage model (B). Cells were treated with the 10 μM of curcumin analogs (sAc1-sAc32), TBHQ, PL and curcumin for 42 h (A), and the cytotoxicity of compounds was determined by the MTT assay. PC12 cells were pre-incubated with curcumin and its derivatives sAc1-sAc32 (10 μM) for 18 h and then subjected to H_2O_2 (640 μM) for 24 h. The protection of compounds finally determined by the MTT assay and the viability of untreated cells (with 60% DMSO) is defined as 100%. Data are expressed as the mean ± SD, n = 3. $^{\#\#\#\#}p < 0.0001$ vs DMSO, ****p□0.0001, ***p□0.001, $^{**}p < 0.01$, $^{*}p < 0.05$ vs H_2O_2.

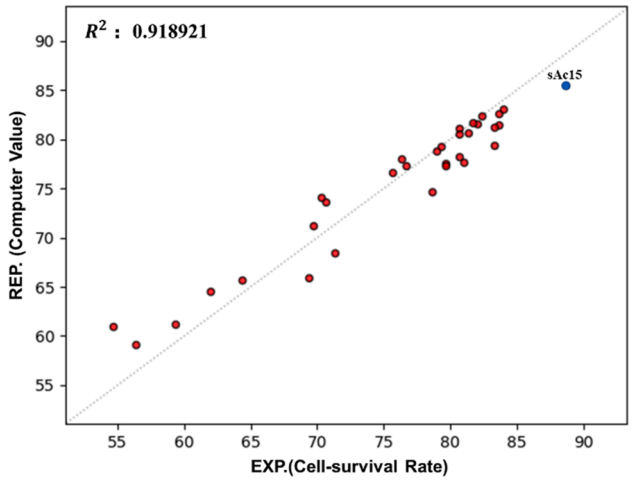

Fig. 3. QSAR model of sAc15 and related on the cell-survival rate. The QSAR model of cell-survival rate of PC12 cells was constructed by RF, which was based on the molecular descriptors of physical and chemical properties and molecular structure.

Imbalance in the production and clearance of ROS leads to oxidative stress, which will destroy proteins, enzymes, lipids and other cellular components, and form the lipid-peroxidation product malondialdehyde (MDA). MDA test results shown in Fig. 4C reveal that MDA contents in the H_2O_2-damaged group were appreciably higher than that in the solvent group. After pre-incubation with **sAc15** for 18 h, the MDA content decreased significantly. When cells are stimulated by H_2O_2, a "burst" of ROS occurs [43]. Compound **sAc15** had an inhibitory effect on excessive ROS generation in cells caused by H_2O_2-induced oxidation. The ROS level was measured by dichloro-dihydro-fluorescein diacetate (DCFH-DA) assay. ROS levels in PC12 cells exposed to H_2O_2 were significantly increased compared with those in the DMSO group (Fig. 4D, E). Pre-treatment with **sAc15** for 18 h eliminated intracellular ROS in a dose-dependent manner, and the fluorescence intensity of **sAc15** at 5 μM was similar to that of TBHQ at the same concentration.

2.5. *sAc15 increased HO-1 protein expression and exerted antioxidant properties by activating the Nrf2 signaling pathway*

Compound **sAc15** exhibited excellent antioxidant properties, so its mechanism of action was further explored. Nrf2 is a "master" regulator of oxidative damage to cells [8]. Therefore, an immunofluorescence assay was used to ascertain if **sAc15** could promote Nrf2 accumulation in nuclei. Blue and red staining represent nuclei and Nrf2, respectively, in Fig. 5A. Compared with the DMSO group, red fluorescence appeared in cell nuclei of the **sAc15** treatment group, and was stronger than that of the positive control group (TBHQ). These results suggested that **sAc15** could promote Nrf2 accumulation in nuclei. During oxidative stress, Nrf2 is activated to induce downstream expression of heme oxygenase-1 (HO-1) and other antioxidant enzymes, which protect cells through anti-inflammatory and anti-oxidation mechanisms, and apoptosis regulation [44]. Next, the effect of **sAc15** on expression of HO-1 protein in PC12 cells was evaluated. Increased expression of the antioxidant enzyme HO-1 was observed in cells incubated with **sAc15**; moreover, with increasing concentrations of **sAc15**, higher expression of HO-1 protein was documented (Fig. 5B). To further confirm the protective effect of compound **sAc15** on cells damaged by H_2O_2-induced oxidative stress, expression of Nrf2 protein was downregulated by transfecting Nrf2 small interfering (si)RNA into PC12 cells (Fig. 5D). The protection elicited by **sAc15** against oxidative-stress damage was evaluated for cells in Nrf2 siRNA and control siRNA groups. Downregulation of Nrf2 expression

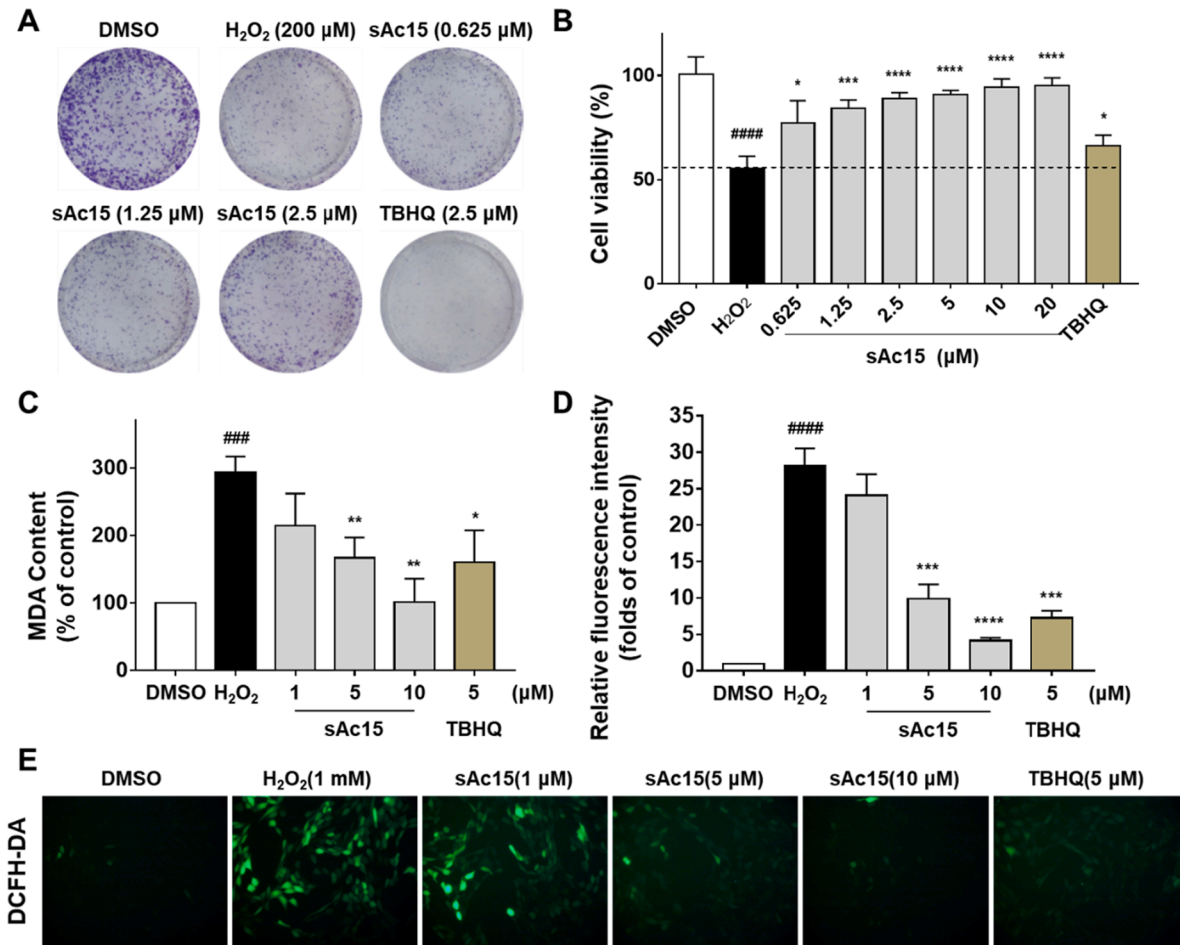

Fig. 4. Protective effects of sAc15 against H_2O_2-induced oxidative stress damage in PC12 cells. (A) Compound sAc15 promoted the colony formation of PC12 cells after exposed to H_2O_2. PC12 cells were pretreated with sAc15 (0.625, 1.25 and 2.5 μM) and TBHQ (2.5 μM) for 18 h, and then incubated with H_2O_2 (200 μM) for 8 days. (B) Compound sAc15 protected PC12 cells from H_2O_2-induced cell damage in a dose-dependent manner. PC12 cells were pre-incubated with TBHQ (20 μM) and sAc15 in different doses (0.625, 1.25, 2.5, 5, 10 and 20 μM) for 18 h. Then, cells were stimulated with H_2O_2 (650 μM) for 24 h. The MTT assay was used to detect the cell viability and the viability of untreated cells (with 60% DMSO) is defined as 100%. PC12 cells were incubated with sAc15 (1, 5 and 10 μM) and TBHQ (5 μM) for 18 h, then treated with H_2O_2(1 mM) for 6 h (C) or 2 h (D, E). The MDA levels (C) and the level of intracellular ROS (D, E) were determined according to the manufacturer's instructions. Data are expressed as the mean ± SD, n = 3. $^{\#\#\#\#}p < 0.0001$, $^{\#\#\#}p < 0.001$ vs DMSO, $^{****}p < 0.0001$, $^{***}p < 0.001$, $^{**}p < 0.01$, $^{*}p < 0.05$ vs H_2O_2.

inhibited the protective effect of **sAc15** (Fig. 5C). Thus, **sAc15** could protect PC12 cells from oxidative damage by targeting Nrf2 to enhance HO-1 expression.

2.6. *sAc15* alleviated brain injury after ischemia–reperfusion in mice

In view of the excellent cytoprotective effect of compound **sAc15** *in vitro*, the neuroprotective effect of **sAc15** *in vivo* was investigated further using mice. Middle cerebral artery occlusion (MCAO), a common model of focal cerebral ischemia, is widely used to study the pathogenesis of cerebral ischemia and screen for therapeutic drugs because its pathogenesis is similar to that of ischemic stroke in humans [45]. Butylphthalide (NBP) is widely used in patients with acute ischemic stroke, the neuroprotective effects of compound **sAc15** and NBP on mice were assessed by intraperitoneal injection before MCAO. Brain slices from the sham-operated group had no infarcted tissue, whereas the prevalence of infarction in the model group brain tissue was ~ 30% (Fig. 6A–C). There was no statistically significant difference in cerebral infarction rates between the vehicle group and the model group, indicating that the solvent itself had no neuroprotective effect. Areas of infarction in the administration group (**sAc15** and NBP) were reduced markedly compared with those in model or solvent groups, and neurological scores were remarkably improved. Hence, the active compound **sAc15** had a good neuroprotective effect against cerebral ischemia.

3. Conclusions

In the current study, a green, simple, and economical synthetic method using edible proline as a catalyst was adopted. This method is suitable for synthesis of monoenone monocarbonyl curcumin analogs with either cyclopentanone or acetone as the bridged ketone, and different substituent groups on the benzene ring.

To improve the stability of curcumin and retain its pharmacological activities, extensive studies have explored a large number of obtained derivatives. Among them, DMCAs are considered promising derivatives that can overcome the defects of curcumin. In the present study, a series of monoenone monocarbonyl curcumin analogs with better prospects for drug development were identified and found to have greater stability, lower toxicity, and stronger antioxidant activity compared with DMCAs.

The vast majority of the 32 analogs did not generate prominent toxicity in PC12 cells at 10 μM. Moreover, various sAc derivatives with distinguished antioxidant protective effects were identified by screening with a model of H_2O_2-induced oxidation damage in PC12 cells. Among these analogs, the optimally active compound **sAc15**, which exhibited far stronger activity than the positive drug TBHQ, was acquired. Our

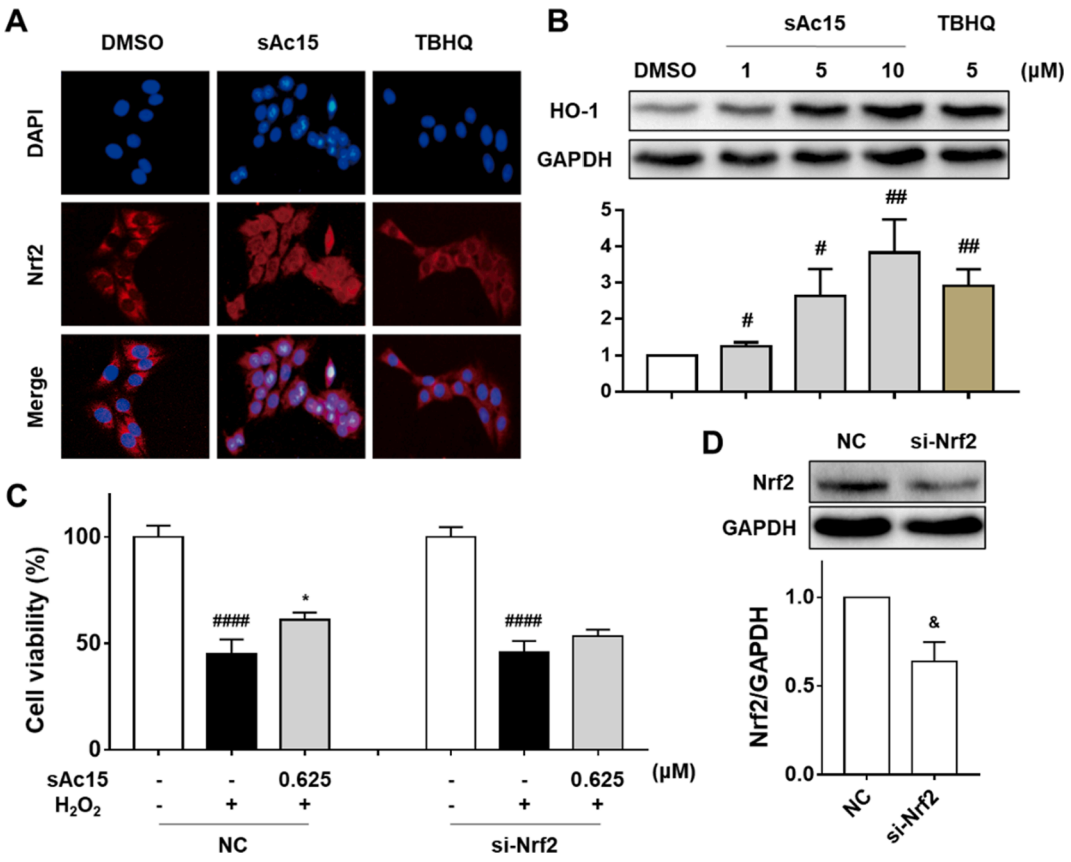

Fig. 5. Compound sAc15 protects PC12 cells against oxidative stress damage by activating the Nrf2 signaling pathway. (A) Compound sAc15 induced Nrf2 nuclei translocation in PC12 cells. After incubation with sAc15 (10 μM) and TBHQ (5 μM) for 6 h, Nrf2 antibody was incubated and DAPI staining was used. The nuclei translocation images were taken under a fluorescence microscope. (B) Compound sAc15 up-regulated the protein expression of HO-1 in PC12 cells. The cells were incubated with sAc15 (1, 5 and 10 μM) and TBHQ (5 μM) for 18 h, and the level of HO-1 protein was measured by western blot assay. (C, D) The cytoprotection of sAc15 weakened after down-regulated the level of Nrf2 protein by siRNA. PC12 cells were transfected respectively with Nrf2 siRNA (si-Nrf2) and control siRNA (NC), pretreated with sAc15 (0.625 μM) for 18 h, and then exposed to H_2O_2 (650 μM) for another 24 h. The cell viability was determined by MTT assay and the protein levels were analyzed by western blot assay. Data are expressed as the mean ± SD, n = 3. $^{\#\#\#\#}p < 0.0001$, $^{\#\#}p$□0.01, $^{\#}p$□0.05 vs DMSO, $^{*}p < 0.05$ vs H_2O_2, $^{\&}p$□0.05 vs NC.

results revealed that **sAc15** could significantly increase the viability of PC12 cells damaged by H_2O_2, even at 0.625 μM. Moreover, **sAc15** could dramatically promote colony formation, suppress MDA production, and reduce intracellular ROS accumulation in PC12 cells damaged by H_2O_2-induced oxidative stress. Furthermore, **sAc15** markedly activated the Nrf2 signaling pathway and promoted Nrf2 translocation into nuclei to upregulate expression of the antioxidant protein HO-1, whereas its protective antioxidant effect on cells almost disappeared when Nrf2 expression was silenced by siRNA. In addition, 2,3,5-triphenyltetrazolium chloride staining of MCAO model mice showed that **sAc15** could effectively decrease the area of cerebral infarction.

In summary, a group of stable, low-toxicity curcumin analogs with outstanding antioxidant activity were synthesized by an environmentally friendly and economical method, and screened. The optimally active compound **sAc15** could effectively scavenge ROS and MDA generated from oxidative-stress damage by activating the Nrf2/HO-1 antioxidant signaling pathway, and exhibited excellent antioxidant activity *in vitro*. Moreover, **sAc15** showed a strong protective effect against CIRI *in vivo*. Overall, our findings show that **sAc15** could emerge as a novel antioxidant candidate drug, as well as a promising chemotherapeutic agent, for the further development of CIRI treatment.

4. Experimental

4.1. Chemistry

Chemical materials and reagents were commercially purchased from Sigma Aldrich (St Louis, Missouri, USA), Aladdin (Shanghai, China), and no further purification was carried out. Reaction progress was monitored with thin-layer chromatography (TLC) making of silica gel GF254. The chromatograms were performed on silica gel (200–300 mesh) and observed under UV light. In addition, melting points (mp) were measured with open capillary tubes on a Fisher-Johns melting apparatus without correction. Mass spectra (MS) were acquired on the Agilent 1100 LC-MS device (Agilent, Palo Alto, CA, USA). ^{1}H NMR spectra were recorded on the 600 MHz spectrometer (Bruker Corporation, Switzerland) with tetramethylsilane (TMS) as an internal standard substance and $CDCl_3$ or DMSO-d_6 as solvent. Coupling constants (J) are expressed in Hz, and splitting patterns are explained as follows: s = singlet; d = doublet; t = triplet; m = multiplet; dd = doublet of doublets; dt = doublet of triplets.

The spectral data of compounds are listed as follows:

4.1.1. (E)-4-phenylbut-3-en-2-one (sAc1)

Yellow powder, 70% yield, mp 34.8–36.0 □ [35-36 □,[46]]. ^{1}H NMR (600 MHz, $CDCl_3$), δ: 7.558–7.542 (m, 2H, Ar-H^2, β-H), 7.520 (d, J = 16.2 Hz, 1H, Ar-H^6), 7.409–7.398 (m, 3H, Ar-H^3, Ar-H^4, Ar-H^5), 6.725 (d, J = 16.2 Hz, 1H, α-H), 2.390 (s, 3H, CH_3). LC-MS m/z: 147.08 (M +

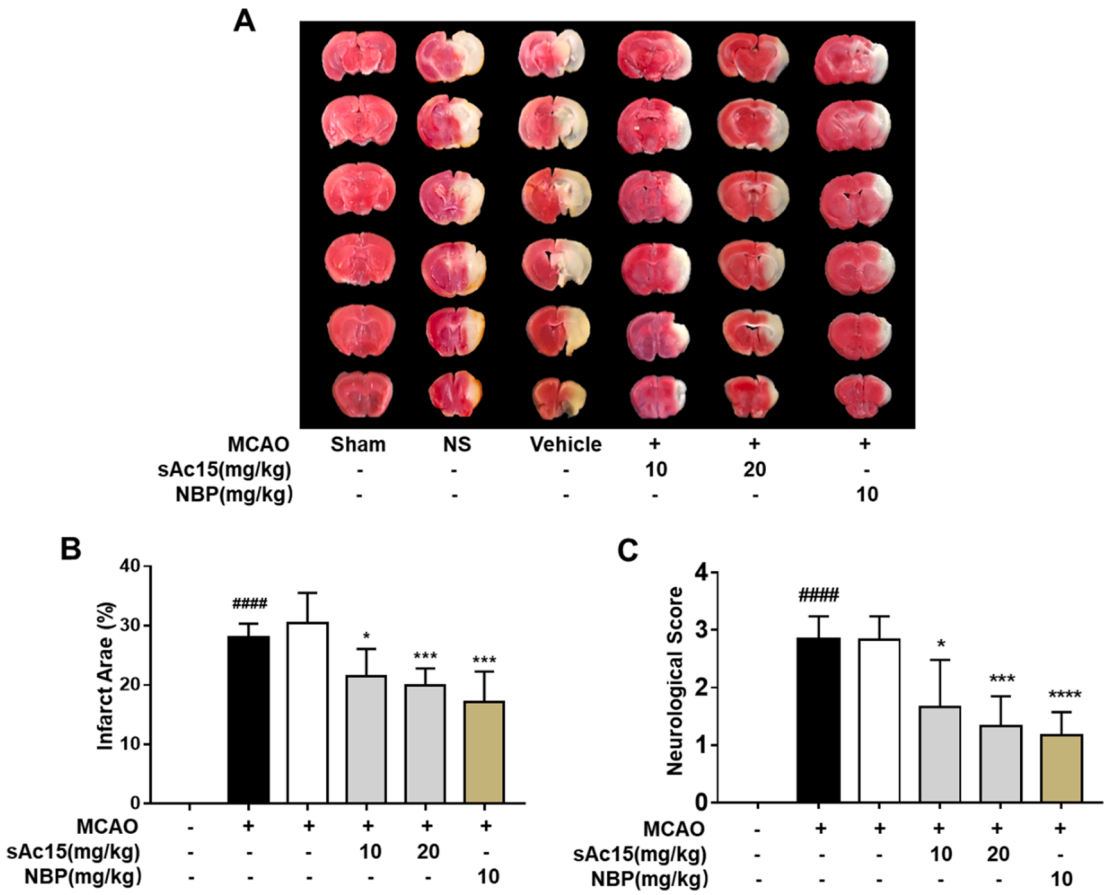

Fig. 6. Compound **sAc15** showed pre-protective effect on mice brain tissue after MCAO. (A) Representative images of TTC-stained brain sections from different experimental groups. (B) Infarct areas (%) levels and neurological score (C) of each group. The sham-operated (Sham) mice or MCAO reperfusion mice received normal saline (NS), vehicle (DMSO: cremophor: normal saline = 1: 19: 80), **sAc15** (10 or 20 mg/kg) and BNP (10 mg/kg) respectively by intraperitoneal injection. Data are expressed as the mean ± SD, n ≥ 6. $^{####}p < 0.0001$ represent the statistical difference between NS and sham-operated group, $^{****}p$□0.0001, $^{***}p < 0.001$, $^{*}p < 0.05$ represent the statistical difference between vehicle-treated and the medicated group.

H)$^+$, calcd for $C_{10}H_{10}O$: 146.07.

4.1.2. (E)-4-(2-methoxyphenyl)but-3-en-2-one (sAc2)

Yellow powder, 66% yield, mp 43.9–45.7 □ [liquid,[46]]. ^{1}H NMR (600 MHz, DMSO-d_6), δ: 7.770 (d, J = 16.2 Hz, 1H, β-H), 7.682 (t, J = 6.6 Hz, 1H, Ar-H^6), 7.425–7.396 (m, 1H, Ar-H^4), 7.086 (d, J = 8.4 Hz, 1H, Ar-H^3), 6.983 (t, J = 7.2 Hz, 1H, Ar-H^5), 6.821 (d, J = 16.8 Hz, 1H, α-H), 3.859 (s, 3H, 2-OCH_3), 2.293 (s, 3H, CH_3). LC-MS *m/z*: 177.09 (M + H)$^+$, calcd for $C_{11}H_{12}O_2$: 176.08.

4.1.3. (E)-4-(3-methoxyphenyl)but-3-en-2-one (sAc3)

Orange oil, 68% yield [liquid,[46]]. ^{1}H NMR (600 MHz, DMSO-d_6), δ: 7.578 (d, J = 16.2 Hz, 1H, β-H), 7.330 (t, J = 8.4 Hz, 1H, Ar-H^5), 7.264 (d, J = 7.2 Hz, 2H, Ar-H^2, Ar-H^6), 6.983 (t, J = 7.8 Hz, 1H, Ar-H^4), 6.814 (d, J = 16.8 Hz, 1H, α-H), 3.780 (s, 3H, 3-OCH_3), 2.317 (s, 3H, CH_3). LC-MS *m/z*: 177.09 (M + H)$^+$, calcd for $C_{11}H_{12}O_2$: 176.08.

4.1.4. (E)-4-(4-methoxyphenyl)but-3-en-2-one (sAc4)

Yellow powder, 71% yield, mp 67.4–68.2 □ [75-78 □,[46]]. ^{1}H NMR (600 MHz, $CDCl_3$), δ: 7.505–7.463 (m, 3H, Ar-H^2, Ar-H^6, β-H), 6.917 (d, J = 8.4 Hz, 2H, Ar-H^3, Ar-H^5), 6.608 (t, J = 7.2 Hz, 1H, α-H), 3.838 (d, J = 7.2 Hz, 3H, 4-OCH_3), 2.354 (d, J = 7.2 Hz, 3H, CH_3). LC-MS *m/z*: 177.09 (M + H)$^+$, calcd for $C_{11}H_{12}O_2$: 176.08.

4.1.5. (E)-4-(2,3-dimethoxyphenyl)but-3-en-2-one (sAc5)

Yellow oil, 65% yield. ^{1}H NMR (600 MHz, DMSO-d_6), δ: 7.724 (d, J = 16.2 Hz, 1H, β-H), 7.315 (dd, J = 1.8 Hz, J = 4.8 Hz, 1H, Ar-H^6), 7.114 (d, J = 2.4 Hz, 2H, Ar-H^4, Ar-H^5), 6.815 (d, J = 16.8 Hz, 1H, α-H), 3.814 (s, 3H, 2-OCH_3), 3.762 (s, 3H, 3-OCH_3), 2.317 (s, 3H, CH_3). LC-MS *m/z*: 207.10 (M+H)$^+$, calcd for $C_{12}H_{14}O_3$: 206.09.

4.1.6. (E)-4-(2,4-dimethoxyphenyl)but-3-en-2-one (sAc6)

White powder, 67% yield, mp 56.1–57.2 □ [58.5-59.5 □,[47]]. ^{1}H NMR (600 MHz, $CDCl_3$), δ: 7.806 (d, J = 16.2 Hz, 1H, Ar-H^6), 7.487 (d, J = 9.0 Hz, 1H, β-H), 6.675 (d, J = 16.2 Hz, 1H, Ar-H^5), 6.517 (dd, J = 2.4 Hz, J = 6.6 Hz, 1H, Ar-H^3), 6.455 (d, J = 2.4 Hz, 1H, α-H), 3.877 (s, 3H, 2-OCH_3), 3.844 (s, 3H, 4-OCH_3), 2.360 (s, 3H, CH_3). LC-MS *m/z*: 207.10 (M + H)$^+$, calcd for $C_{12}H_{14}O_3$: 206.09.

4.1.7. (E)-4-(2,5-dimethoxyphenyl)but-3-en-2-one (sAc7)

Yellow powder, 64% yield, mp 41.2–42.1 □ [49-51 □,[48]]. ^{1}H NMR (600 MHz, $CDCl_3$), δ: 7.859 (d, J = 16.2 Hz, 1H, β-H), 7.076 (d, J = 3.0 Hz, 1H, Ar-H^3), 6.931 (dd, J = 3.0 Hz, J = 6.0 Hz, 1H, Ar-H^6), 6.859 (d, J = 9.0 Hz, 1H, Ar-H^4), 6.713 (d, J = 16.2 Hz, 1H, α-H), 3.855 (s, 3H, 2-OCH_3), 3.791 (s, 3H, 5-OCH_3), 2.391 (s, 3H, CH_3). LC-MS *m/z*: 207.10 (M + H)$^+$, calcd for $C_{12}H_{14}O_3$: 206.09.

4.1.8. (E)-4-(3,4-dimethoxyphenyl)but-3-en-2-one (sAc8)

Yellow powder, 61% yield, mp 78.1–79.9 □ [81-82 □,[49]]. ^{1}H NMR (600 MHz, DMSO-d_6), δ: 7.541 (d, J = 16.2 Hz, 1H, β-H), 7.305 (d, J = 1.2 Hz, 1H, Ar-H^2), 7.236 (dd, J = 1.2 Hz, J = 7.2 Hz, 1H, Ar-H^5), 6.986 (d, J = 8.4 Hz, 1H, Ar-H^6), 6.720 (d, J = 16.2 Hz, 1H, α-H), 3.785 (d, J = 6.0 Hz, 6H, 3-OCH_3, 4-OCH_3), 2.287 (s, 3H, CH_3). LC-MS *m/z*: 207.10 (M + H)$^+$, calcd for $C_{12}H_{14}O_3$: 206.09.

4.1.9. (E)-4-(3,5-dimethoxyphenyl)but-3-en-2-one (sAc9)

White powder, 67% yield, mp 68.5–69.4 □ [70-72 □,[50]]. ^{1}H NMR (600 MHz, DMSO-d_6), δ: 7.529 (d, J = 16.2 Hz, 1H, β-H), 6.873 (d, J = 1.8 Hz, 2H, Ar-H^2, Ar-H^6), 6.820 (d, J = 16.8 Hz, 1H, α-H), 6.542 (s, 1H, Ar-H^4), 3.761 (s, 6H, 3-OCH_3, 5-OCH_3), 2.310 (s, 3H, CH_3). LC-MS m/z: 207.10 $(M + H)^+$, calcd for $C_{12}H_{14}O_3$: 206.09.

4.1.10. (E)-4-(2,4,5-trimethoxyphenyl)but-3-en-2-one (sAc10)

White powder, 59% yield, mp 94.5–95.0 □ [106-108 □,[51]]. ^{1}H NMR (600 MHz, $CDCl_3$), δ: 7.732 (d, J = 16.2 Hz, 1H, β-H), 7.225 (s, 1H, α-H), 6.734 (t, J = 16.2 Hz, 2H, Ar-H^3, Ar-H^5), 3.839 (d, J = 11.4 Hz, 6H, 2-OCH_3, 5-OCH_3), 3.733 (s, 3H, 4-OCH_3), 2.251 (s, 3H, CH_3). LC-MS m/z: 237.11 $(M + H)^+$, calcd for $C_{13}H_{16}O_4$: 236.10.

4.1.11. (E)-4-(2,4,6-trimethoxyphenyl)but-3-en-2-one (sAc11)

Yellow powder, 57% yield, mp 116.8–117.6 □ [116.8-117.6□,[51]]. ^{1}H NMR (600 MHz, $CDCl_3$), δ: 7.937 (d, J = 16.8 Hz, 1H, β-H), 7.063 (d, J = 16.8 Hz, 1H, α-H), 6.115 (s, 2H, Ar-H^3, Ar-H^5), 3.858 (d, J = 15.6 Hz, 9H, 2-OCH_3, 4-OCH_3, 6-OCH_3), 2.343 (s, 3H, CH_3). LC-MS m/z: 237.11 $(M + H)^+$, calcd for $C_{13}H_{16}O_4$: 236.10.

4.1.12. (E)-4-(3,4,5-trimethoxyphenyl)but-3-en-2-one (sAc12)

White powder, 57% yield, mp 87.0–88.1 □ [84-85 □,[52]]. ^{1}H NMR (600 MHz, $CDCl_3$), δ: 7.433 (d, J = 16.2 Hz, 1H, β-H), 6.775 (s, 2H, Ar-H^2, Ar-H^6), 6.631 (d, J = 16.2 Hz, 1H, α-H), 3.893 (d, J = 4.2 Hz, 9H, 3-OCH_3, 4-OCH_3, 5-OCH_3), 2.384 (s, 3H, CH_3). LC-MS m/z: 237.11 $(M + H)^+$, calcd for $C_{13}H_{16}O_4$: 236.10.

4.1.13. (E)-4-(3-hydroxyphenyl)but-3-en-2-one (sAc13)

White powder, 50% yield, mp 91.3–92.1 □ [94-95 □,[53]]. ^{1}H NMR (600 MHz, DMSO-d_6), δ: 9.654 (s, 1H, 3-OH), 7.508 (d, J = 16.2 Hz, 1H, β-H), 7.214 (t, J = 7.8 Hz, 1H, Ar-H^5), 7.110 (d, J = 7.8 Hz, 1H, Ar-H^6), 7.025 (s, 1H, Ar-H^4), 6.819 (dd, J = 1.2 Hz, J = 6.6 Hz, 1H, Ar-H^2), 6.665 (d, J = 16.2 Hz, 1H, α-H), 2.304 (s, 3H, CH_3). LC-MS m/z: 163.07 $(M + H)^+$, calcd for $C_{10}H_{10}O_2$: 162.07.

4.1.14. (E)-4-(4-hydroxyphenyl)but-3-en-2-one (sAc14)

Yellow powder, 48% yield, mp 83.2–85.5 □ [102.1-104.8 □,[54]]. ^{1}H NMR (600 MHz, $CDCl_3$), δ: 7.495 (d, J = 16.2 Hz, 1H, β-H), 7.453 (dt, J = 8.4 Hz, J = 9.6 Hz, 2H, Ar-H^2, Ar-H^6), 6.889 (dd, J = 1.8 Hz, J = 4.8 Hz, 2H, Ar-H^3, Ar-H^5), 6.609 (d, J = 16.2 Hz, 1H, α-H), 2.383 (s, 3H, CH_3). LC-MS m/z: 163.07 $(M + H)^+$, calcd for $C_{10}H_{10}O_2$: 162.07.

4.1.15. (E)-4-(3,4-dihydroxyphenyl)but-3-en-2-one (sAc15)

Brown powder, 45% yield, mp 162.8–164.0 □ [173-175 □,[53]]. ^{1}H NMR (600 MHz, DMSO-d_6), δ: 9.587 (s, 1H, 3-OH), 9.159 (s, 1H, 4-OH), 7.432 (d, J = 16.2 Hz, 1H, β-H), 7.042 (d, J = 1.8 Hz, 1H, Ar-H^2), 6.990 (dd, J = 1.8 Hz, J = 6.6 Hz, 1H, Ar-H^5), 6.758 (d, J = 8.4 Hz, 1H, Ar-H^6), 6.462 (d, J = 16.2 Hz, 1H, α-H), 2.258 (s, 3H, CH_3). LC-MS m/z: 179.07 $(M + H)^+$, calcd for $C_{10}H_{10}O_3$: 178.06.

4.1.16. (E)-4-(3-hydroxy-4-methoxyphenyl)but-3-en-2-one (sAc16)

Beige powder, 52% yield, mp 84.0–85.5 □ [74-76 □,[53]]. ^{1}H NMR (600 MHz, $CDCl_3$), δ: 7.428 (d, J = 16.2 Hz, 1H, β-H), 7.155 (d, J = 2.4 Hz, 1H, Ar-H^2), 7.059 (dd, J = 2.4 Hz, J = 6.0 Hz, 1H, Ar-H^5), 6.861 (d, J = 7.8 Hz, 1H, Ar-H^6), 6.588 (d, J = 16.2 Hz, 1H, α-H), 3.936 (s, 3H, 4-OCH_3), 2.358 (s, 3H, CH_3). LC-MS m/z: 193.08 $(M + H)^+$, calcd for $C_{11}H_{12}O_3$: 192.08.

4.1.17. (E)-4-(4-hydroxy-3-methoxyphenyl)but-3-en-2-one (sAc17)

Beige powder, 56% yield, mp 115.9–117.8 □ [125.3-126.6 □,[54]]. ^{1}H NMR (600 MHz, $CDCl_3$), δ: 7.451 (d, J = 16.2 Hz, 1H, β-H), 7.093 (dd, J = 1.8 Hz, J = 6.6 Hz, 1H, Ar-H^2), 7.060 (d, J = 1.8 Hz, 1H, Ar-H^5), 6.935 (d, J = 8.4 Hz, 1H, α-H), 6.589 (d, J = 16.2 Hz, 1H, Ar-H^6), 3.937 (s, 3H, 3-OCH_3), 2.368 (s, 3H, CH_3). LC-MS m/z: 193.08 $(M + H)^+$, calcd for $C_{11}H_{12}O_3$: 192.08.

4.1.18. (E)-4-(4-hydroxy-3,5-dimethoxyphenyl)but-3-en-2-one (sAc18)

Beige powder, 44% yield, mp 131.2–132.5 □ [132.5-134.5 □,[55]]. ^{1}H NMR (600 MHz, $CDCl_3$), δ: 7.429 (d, J = 16.2 Hz, 1H, β-H), 6.794 (s, 2H, Ar-H^2, Ar-H^6), 6.597 (d, J = 16.2 Hz, 1H, α-H), 3.926 (s, 6H, 3-OCH_3, 5-OCH_3), 2.369 (s, 3H, α-CH_3). LC-MS m/z: 223.09 $(M + H)^+$, calcd for $C_{12}H_{14}O_4$: 222.09.

4.1.19. (E)-3-(3-oxobut-1-en-1-yl)benzaldehyde (sAc19)

White powder, 40% yield, mp 47.9–48.8 □. ^{1}H NMR (600 MHz, $CDCl_3$), δ: 10.052 (s, 1H, 3-CHO), 8.048 (t, J = 1.8 Hz, 1H, Ar-H^6), 7.905 (dt, J = 7.8 Hz, J = 7.2 Hz, 1H, Ar-H^4), 7.798 (dd, J = 1.2 Hz, J = 6.6 Hz, 1H, β-H), 7.601–7.547 (m, 2H, Ar-H^2, Ar-H^5), 6.809 (d, J = 16.2 Hz, 1H, α-H), 2.406 (s, 3H, CH_3). LC-MS m/z: 175.07 $(M + H)^+$, calcd for $C_{11}H_{10}O_2$: 174.07.

4.1.20. (E)-4-(3-fluorophenyl)but-3-en-2-one (sAc20)

Yellow oil, 57% yield [liquid,[46]]. ^{1}H NMR (600 MHz, DMSO-d_6), δ: 7.604 (t, J = 4.2 Hz, 2H, β-H, Ar-H^6), 7.537 (d, J = 7.2 Hz, 1H, Ar-H^5), 7.481–7.444 (m, 1H, Ar-H^4), 7.266–7.235 (m, 1H, Ar-H^2), 6.863 (d, J = 16.2 Hz, 1H, α-H), 2.322 (s, 3H, CH_3). LC-MS m/z: 165.07 $(M + H)^+$, calcd for $C_{10}H_9FO$: 164.06.

4.1.21. (E)-4-(4-fluorophenyl)but-3-en-2-one (sAc21)

Yellow oil, 60% yield [38-40 □,[46]]. ^{1}H NMR (600 MHz, DMSO-d_6), δ: 7.788–7.764 (m, 2H, Ar-H^3, Ar-H^5), 7.613 (d, J = 16.8 Hz, 1H, β-H), 7.261 (t, J = 9.0 Hz, 2H, Ar-H^2, Ar-H^6), 6.762 (d, J = 16.2 Hz, 1H, α-H), 2.312 (s, 3H, CH_3). LC-MS m/z: 165.07 $(M + H)^+$, calcd for $C_{10}H_9FO$: 164.06.

4.1.22. (E)-4-(3,4-difluorophenyl)but-3-en-2-one (sAc22)

Yellow oil, 51% yield [39 □,[56]]. ^{1}H NMR (600 MHz, DMSO-d_6), δ: 7.893–7.860 (m, 1H, β-H), 7.578 (d, J = 16.8 Hz, 2H, Ar-H^5, Ar-H^6), 7.491 (d, J = 10.2 Hz, 1H, Ar-H^2), 6.829 (d, J = 16.2 Hz, 1H, α-H), 2.310 (s, 3H, CH_3). LC-MS m/z: 183.06 $(M + H)^+$, calcd for $C_{10}H_8F_2O$: 182.05.

4.1.23. (E)-4-(3,5-difluorophenyl)but-3-en-2-one (sAc23)

Yellow oil, 55% yield [58 □,[56]]. ^{1}H NMR (600 MHz, DMSO-d_6), δ: 7.572 (d, J = 16.2 Hz, 1H, β-H), 7.501 (d, J = 6.6 Hz, 2H, Ar-H^2, Ar-H^6), 7.312–7.282 (m, 1H, α-H), 6.928 (d, J = 16.2 Hz, 1H, Ar-H^4), 2.319 (s, 3H, CH_3). LC-MS m/z: 183.06 $(M + H)^+$, calcd for $C_{10}H_8F_2O$: 182.05.

4.1.24. (E)-4-(3-chlorophenyl)but-3-en-2-one (sAc24)

Yellow oil, 56% yield [36 □,[57]]. ^{1}H NMR (600 MHz, DMSO-d_6), δ: 7.812 (s, 1H, β-H), 7.671 (d, J = 7.2 Hz, 1H, Ar-H^6), 7.587 (d, J = 16.2 Hz, 1H, Ar-H^5), 7.477–7.430 (m, 2H, Ar-H^2, Ar-H^4), 6.880 (d, J = 16.2 Hz, 1H, α-H), 2.319 (s, 3H, CH_3). LC-MS m/z: 181.04 $(M + H)^+$, calcd for $C_{10}H_9ClO$: 180.03.

4.1.25. (E)-4-(4-chlorophenyl)but-3-en-2-one (sAc25)

White powder, 61% yield, mp 51.6–52.2 □ [63-65 □,[46]]. ^{1}H NMR (600 MHz, $CDCl_3$), δ: 7.485–7.448 (m, 3H, Ar-H^2, Ar-H^6, β-H), 7.387–7.365 (m, 2H, Ar-H^3, Ar-H^5), 6.689 (d, J = 16.2 Hz, 1H, α-H), 2.382 (s, 3H, CH_3). LC-MS m/z: 181.04 $(M + H)^+$, calcd for $C_{10}H_9ClO$: 180.03.

4.1.26. (E)-4-(3,5-dichlorophenyl)but-3-en-2-one (sAc26)

White powder, 57% yield, mp 72.0–72.5 □. ^{1}H NMR (600 MHz, $CDCl_3$), δ: 7.407 (d, J = 1.8 Hz, 2H, β-H, Ar-H^4), 7.367 (t, J = 1.8 Hz, 2H, Ar-H^2, Ar-H^6), 6.700 (d, J = 16.2 Hz, 1H, α-H), 2.379 (s, 3H, CH_3). LC-MS m/z: 215.99 $(M + H)^+$, calcd for $C_{10}H_8Cl_2O$: 214.00.

4.1.27. (E)-4-(4-bromophenyl)but-3-en-2-one (sAc27)

White powder, 62% yield, mp 74.9–76.4 □ [46-48 □,[46]]. ^{1}H NMR (600 MHz, $CDCl_3$), δ: 7.532 (d, J = 8.4 Hz, 2H, Ar-H^3, Ar-H^5), 7.442 (d, J = 16.2 Hz, 1H, β-H), 7.405 (d, J = 8.4 Hz, 2H, Ar-H^2, Ar-H^6), 6.700 (d, J = 16.2 Hz, 1H, α-H), 2.376 (s, 3H, CH_3). LC-MS m/z: 224.99 $(M + H)^+$,

calcd for $C_{10}H_9BrO$: 223.98.

4.1.28. (E)-4-(4-(dimethylamino)phenyl)but-3-en-2-one (sAc28)

Yellow powder, 61% yield, mp 129.7–130.7 □ [135-137 □,[58]]. ^1H NMR (600 MHz, $CDCl_3$), δ: 7.453 (t, $J = 16.8$ Hz, 3H, Ar-H^2, Ar-H^6, β-H), 6.678 (d, $J = 8.4$ Hz, 2H, Ar-H^3, Ar-H^5), 6.546 (d, $J = 16.8$ Hz, 1H, α-H), 3.031 (s, 6H, 4-$N(CH_3)_2$), 2.340 (s, 3H, CH_3). LC-MS *m/z*: 190.12 $(M + H)^+$, calcd for $C_{12}H_{15}NO$: 189.12.

4.1.29. (E)-4-(4-(diethylamino)phenyl)but-3-en-2-one (sAc29)

Yellow oil, 58% yield. ^1H NMR (600 MHz, DMSO-d_6), δ: 7.480–7.451 (m, 3H, Ar-H^2, Ar-H^6, β-H), 6.658 (d, $J = 9.0$ Hz, 2H, Ar-H^3, Ar-H^5), 6.485 (d, $J = 16.2$ Hz, 1H, α-H), 3.388–3.353 (m, 4H, $N(CH_2)_2$), 2.235 (s, 3H, CH_3), 1.086 (t, $J = 6.6$ Hz, 6H, $C(CH_3)_2$). LC-MS *m/z*: 218.15 $(M + H)^+$, calcd for $C_{14}H_{19}NO$: 217.15.

4.1.30. (E)-4-(4-(piperidin-1-yl)phenyl)but-3-en-2-one (sAc30)

Yellow powder, 54% yield, mp 98.4–99.4 □. ^1H NMR (600 MHz, DMSO-d_6), δ: 7.490 (t, $J = 8.4$ Hz, 3H, Ar-H^2, Ar-H^6, β-H), 6.913 (d, $J = 9.0$ Hz, 2H, Ar-H^3, Ar-H^5), 6.545 (d, $J = 16.2$ Hz, 1H, α-H), 3.031 (s, 4H, $N(CH_2)_2$), 2.250 (s, 3H, CH_3), 1.557 (s, 6H, $CH_2CH_2CH_2$). LC-MS *m/z*: 230.15 $(M + H)^+$, calcd for $C_{15}H_{19}NO$: 229.15.

4.1.31. (E)-4-(4-morpholinophenyl)but-3-en-2-one (sAc31)

Yellow powder, 51% yield, mp 131.7–132.8 □. ^1H NMR (600 MHz, $CDCl_3$), δ: 7.466–7.415 (m, 3H, Ar-H^2, Ar-H^6, β-H), 6.884 (t, $J = 7.8$ Hz, 2H, Ar-H^3, Ar-H^5), 6.603–6.524 (m, 1H, α-H), 3.841 (d, $J = 30.0$ Hz, 4H, $O(CH_2)_2$), 3.257–3.206 (m, 4H, $N(CH_2)_2$), 2.351–2.298 (m, 3H, CH_3). LC-MS *m/z*: 232.13 $(M + H)^+$, calcd for $C_{14}H_{17}NO_2$: 231.13.

4.1.32. (E)-4-(naphthalen-2-yl)but-3-en-2-one (sAc32)

White powder, 55% yield, mp 97.0–98.3 □ [103-104 □,[59]]. ^1H NMR (600 MHz, $CDCl_3$), δ: 7.965 (s, 1H, Ar-H^3), 7.878–7.836 (m, 3H, Ar-H^2, Ar-H^6, Ar-H^7), 7.698–7.672 (m, 2H, Ar-H^8, β-H), 7.539–7.519 (m, 2H, Ar-H^4, Ar-H^5), 6.842 (d, $J = 16.2$ Hz, 1H, α-H), 2.431 (s, 3H, CH_3). LC-MS *m/z*: 197.09 $(M + H)^+$, calcd for $C_{14}H_{12}O$: 196.09.

4.2. General procedure for synthesis of sAc15 analogs

Taking a reaction flask as reaction vessel, 1 mmol of substituted benzaldehyde and 5 mmol of acetone were dissolved in anhydrous dimethyl sulfoxide (DMSO). Then, 0.2 mmol of L-proline was added to the reaction system as a catalyst, and the mixture was stirred at room temperature overnight. Next, 2–3 drops of condensed HCl were added to the solution, and the reaction was unceasingly stirred at room temperature for 2–3 h. Taking thin layer chromatography (TLC) as a monitoring way, when the endpoint of the reaction was arrived, the mixture was extracted with ethyl acetate/saturated sodium chloride aqueous solution (3 × 20 mL). The organic layer was enriched and dried with anhydrous Na_2SO_4. And a crude product was obtained by concentrated and evaporated the organic layer in vacuo. At last, the pure product was got on a silica gel column and ethyl acetate and petroleum ether were used as eluent.

4.3. Stability test

The certain mass of compound was completely dissolved in a certain volume of dimethyl sulfoxide (DMSO) to get a solution with a concentration of 1 mM, then the concentration of the solution was diluted to 30 μM with phosphate buffer (PBS, PH = 7.4). The optical density (OD) of the diluted solution at a wavelength of 200 to 800 nm was measured by UV–Visible spectrophotometer. Taking 5 min as a time interval and 5 nm as a wavelength interval, every single diluted sample solution was tested for 30 min each time. Then three times independent experiments were conducted to each sample solution and the absorption curve was obtained by data analysis. Finally, the stability of compounds can be evaluated by ultraviolet spectrophotometry.

4.4. Biological evaluation

4.4.1. Cell culture

An adrenal pheochromocytoma cell line from rats (PC12) were purchased from Wuhan University Cell Storage Center (Wuhan, China). The cell lines were cultured in 1 × DMEM (4.5 g/L D-glucose, Gibco, Eggenstein, Germany) complemented with 10% fetal bovine serum (FBS, Gibco) and 1% penicillin/streptomycin. The cells were maintained at 37 °C constant temperature incubators with 5% CO_2 (Thermo Fisher Scientific, Massachusetts, USA).

4.4.2. MTT assay

3-(4,5-dimethyl-2-thiazolyl)-2,5-diphenyl-2H-tetrazolium bromide (MTT; Sigma, St Louis, Missouri, USA) assay also called MTT colorimetry was used to detect the toxicity and the cytoprotection of compounds. In brief, approximate 5×10^3 PC12 cells were plated onto each well of 96-well plates (NEST Biotechnology Co. LTD., Wuxi, China) and incubated at 37 °C in 5% CO_2 for the night. Then, the compounds dissolved in 60% DMSO was added to incubate with cells for 18 h, and H_2O_2 was added to stimulate for 24 h or not. 20 μL MTT (0.5 mg/mL) was added and incubated with cells at 37 °C for 4 h shielded from light. The liquid was then carefully removed and DMSO (120 μL) was added to each well. Finally, the absorbency at 490 nm was measured using a Microplate Reader (Bio-Rad, USA). Every test repeated at least three times.

4.4.3. Cell colony formation assay

The cell colony formation assay is used to assess the proliferation capacity of cells at very low densities. 2000 individual PC12 cells were evenly seeded into 6-well plates and cultured for night. Cells were pre-treated with **sAc15** and TBHQ for 18 h, and the cells were incubated with H_2O_2 (200 μM) continuously for 8 days. Finally, cell colonies were fixed with 4% paraformaldehyde for 30 min and the fixed colony cells were stained using crystal violet for 30 min before dried to be taken photographs.

4.4.4. MDA assay

PC12 cells were seeded on 6-well plates at 3×10^5/well for 24 h, then incubated with compound **sAc15** and TBHQ for 18 h, and then stimulated with H_2O_2 (1 mM) for 6 h. The protein supernatant was collected and reacted with thiobarbituric acid (TBA) to measure the level of MDA. The relative MDA content was calculated strictly according to the method provided by the reagent manufacturer (Beyotime Biotech, China).

4.4.5. Reactive oxygen species assay

The fluorescent probe dichloro-dihydro-fluorescein diacetate (DCFH-DA; Beyotime Biotech, Shanghai, China) was utilized to detect intracellular reactive oxygen species (ROS) formation. The experimental procedures are strictly carried out according to manufacturer's recommendations (Beyotime Biotech). Briefly, 3×10^5 PC12 cells were plated in 6-well plates, allowed to attach for 24 h and then cells were treated with **sAc15** for 18 h and H_2O_2 (1 mM) was carried out for another 2 h. Then cells were incubated with DCFH-DA at a terminal concentration of 10 μM at 37 °C for 30 min in the dark. The images were made in a fluorescence microscope (Nikon).

4.4.6. Immunofluorescence assay

PC12 cells were seeded on 6-well plates at 2×10^5/well, incubated with **sAc15** and TBHQ for 6 h after 24 h, fixed with 4% paraformaldehyde for 20 min, washed with PBS for three times, then treated with 1% Triton X100 (Beyotime Biotech, China) for 15 min, washed with PBS for three times, then sealed with 2% BSA at room temperature for 1 h, and then added Nrf2 antibody (sc-13032, Santa Cruz biotechnology, USA, 1: 200). The next day, washed with PBS for 3 times, and then

incubated with fluorescent mouse antibody (sc-13032, Goat anti mouse IgG PE, Santa Cruz biotechnology, USA, 1: 300) in 37 °C incubator for 1 h. Washed with PBS for 3 times, and then incubated with DAPI (Beyotime Biotech, China) in dark for 8 min. After sealing with neutral resin, the cells photographed under the microscope (Nikon, Japan).

4.4.7. Western blot assay

Western blot assay was used to detect the level of protein expression in cells. At 18 h post incubation with compounds, cells were harvested for western blot. Total protein was extracted with ice-cold RIPA lysis buffer and then was separated by sodium dodecyl sulfate polyacrylamide gel electrophoresis (SDS-PAGE). The separated protein was subsequently transferred to a Polyvinylidene Fluoride (PVDF) membrane (Millipore, Massachusetts, USA), which were blocked at room temperature with 5% skim milk for 1 h and then probed overnight using primary antibodies (HO-1, sc-10789, Santa Cruz Biotechnology, 1:500; anti-GADPH, sc-47724, Santa Cruz Biotechnology, 1:2000) at 4 °C. Next day, the PVDF membranes were incubated with secondary antibodies for 90 min at room temperature. The protein bands were imaged by a ChemiDoc XRS + system (Bio-Rad, Hercules, CA, USA) and measured using Image J software (National Institute of Health, Bethesda, MD, USA).

4.4.8. Transfection assay

The short interfering RNA (siRNA) targeting Nrf2 was provided by Shanghai GenePharma Company (siRNA sequence, sense: 5′-GGUUCAGUGACUCGGAAAUTT-3′, antisense: 5′-AUUUCCGAGUCACUGAACCTT-3′). For the process of transfection, PC12 cells were plated in culture dishes (1 million per dish) and transfection with Nrf2 siRNA was performed using the Lipofectamine™ 2000 Transfection reagent (Invitrogen, Carlsbad, CA, USA) according to the manufacturer's recommendations. During transfection, cells were incubated with the starvation medium to improve the transfection efficiency. 10 h after transfection, the medium containing fetal bovine serum was used to replace the original starvation medium and the transfected cells could be cultured for further experiments.

4.4.9. Experimental animals

All male C57BL/6 mice used for animal experiments were obtained from the Zhejiang Muke Biotechnology Co., Ltd. All mice were fed during a period of adaptive breeding until the weight of the mice reached 23–26 g. All animal experiments are followed the principles of the National Institutes of Health guide for the care and use of Laboratory animals (NIH Publications No.8023, revised 1978).

4.4.10. MCAO-induced cerebral ischemia/reperfusion injury model

All the animals were divided into 6 groups evenly, and the enterocoelia was injected with normal saline, solvent (DMSO: cremophor: normal saline = 1: 19: 80), **sAc15** and butylphthalide (NBP) separately at 1 h before MCAO. Firstly, male B6 mice were narcotized by injecting 1% sodium pentobarbital (50 mg/kg) into their peritoneal cavities, and placed them in the supine position. Secondly, the neck was cut and exposed the right common carotid artery (CCA), external carotid artery (ECA) and the internal carotid artery (ICA). Thirdly, ECA and its small vessels were ligated with thin wires, ICA and CCA were temporarily closed with arterial forceps. In the end, a small incision was made on the ECA ~ 2 mm away from the CCA branch to insert the occlusion line to block the middle cerebral artery. 1 h after MCAO, the nylon monofilament was removed and reperfusion for 48 h. The sham operation group performed the same operation but was not inserted the suture.

4.4.11. Behavioral tests and infarct area calculations

Neurological deficit score of mice was evaluated at 48 h after reperfusion. The scoring criteria are as follows: 0, no symptoms of nerve injury; 1, unable to fully extend contralateral front paws; 2, circle to the paralyzed side; 3, dump to the contralateral side; 4, no spontaneous loco-motor activity, loss of consciousness. For 2,3,5-triphenyltetrazolium chloride (TTC; Sigma, St. Louis, MO, USA) staining, the brain tissue was taken out and frozen at −20 °C for 20 min, and then placed in a brain slice mold and cut into 1 mm continuous sections. After that, the brain slices were stained with 2% of TTC at 37 °C shielded from light until the normal sections were rosy red and the infarcted tissues were white and were fixed with 4% paraformaldehyde. In the end, after brain tissues were completely fixed and the brain slices were photographed, and the infarct size was measured by Image J software (National Institutes of Health, Bethesda, MD, USA).

4.4.12. Quantitative structure–activity relationships analysis

This modeling is based on Python language and SCI learn machine learning library. First of all, we use rdkit to calculate the molecular descriptors of small molecules, which is a basic requirement for building QSAR model. The results include 208 dimensional 2D molecular descriptors, such as molecular weight, topological polarity surface area, lipid water partition coefficient, etc. In these descriptors, the descriptors whose contents are equal and undifferentiated are deleted. After screening, 123 dimensional molecular descriptors were retained. The molecular descriptors are input into the random forest, and the QSAR model is obtained by computer training. In this modeling process, the default number of sub decision trees is 800.

4.4.13. Statistical analysis

The datum was presented as means ± SEM. The statistical differences were analyzed by the unpaired *t* test or ordinary one-way ANOVE. P values <0.05 ($P < 0.05$) were considered as significant differences.

Declaration of Competing Interest

The authors declare that they have no known competing financial interests or personal relationships that could have appeared to influence the work reported in this paper.

Acknowledgement

This work was supported by Zhejiang Province Natural Science Fund of China (Grant Nos. LY19B020012, LQ20H090004), National Natural Science Foundation of China (82003755), National Undergraduate Training Programs for Innovation and Entrepreneurship (201910343026, 201810343025), International (Regional) Cooperation and Exchange Projects of the National Natural Science Foundation of China (81820108011), and the Key Project of Science Technology Department of Zhejiang Province (2017C03027)

We thank Arshad Makhdum, PhD, from Liwen Bianji, Edanz Group China (www.liwenbianji.cn/ac), for editing the English text of a draft of this manuscript.

Appendix A. Supplementary material

Supplementary data to this article can be found online at https://doi.org/10.1016/j.bioorg.2021.105080.

References

[1] S. Seo, S. Choi, K. Kim, S.M. Kim, S.M. Park, Association between urban green space and the risk of cardiovascular disease: A longitudinal study in seven Korean metropolitan areas, Environ. Int. 125 (2019) 51–57.

[2] R. Malik, M. Dichgans, Challenges and opportunities in stroke genetics, Cardiovasc. Res. 114 (2018) 1226–1240.

[3] H. Ma, B.C.V. Campbell, M.W. Parsons, L. Churilov, C.R. Levi, C. Hsu, T.J. Kleinig, T. Wijeratne, S. Curtze, H.M. Dewey, F. Miteff, C.H. Tsai, J.T. Lee, T.G. Phan, N. Mahant, M.C. Sun, M. Krause, J. Sturm, R. Grimley, C.H. Chen, C.-J. Hu, A. A. Wong, D. Field, Y. Sun, P.A. Barber, A. Sabet, J. Jannes, J.S. Jeng, B. Clissold, R. Markus, C.H. Lin, L.M. Lien, C.F. Bladin, S. Christensen, N. Yassi, G. Sharma, A. Bivard, P.M. Desmond, B. Yan, P.J. Mitchell, V. Thijs, L. Carey, A. Meretoja, S. M. Davis, G.A. DonnanMa, Thrombolysis guided by perfusion imaging up to 9 hours after onset of stroke, N. Engl. J. Med. 380 (2019) 1795–1803.

[4] S. Staessens, F. Denorme, O. François, L. Desender, T. Dewaele, P. Vanacker, H. Deckmyn, K. Vanhoorelbeke, T. Andersson, S.F. De Meyer, Structural analysis of ischemic stroke thrombi: histological indications for therapy resistance, Haematologica. 105 (2020) 498–507.
[5] Y. Liu, J.W. Min, S. Feng, K. Subedi, F. Qiao, E. Mammenga, E. Callegari, H. Wang, Therapeutic role of a cysteine precursor, OTC, in ischemic stroke is mediated by iImproved proteostasis in mice, Transl. Stroke. Res. 11 (2020) 147–160.
[6] E. Candelario-Jalil, Injury and repair mechanisms in ischemic stroke: Considerations for the development of novel neurotherapeutics, Current. Opinion. Invest. Drugs. 10 (2009) 644–654.
[7] Y. Song, L.B. Wang, Y. Bei, D.X. Qin, L.Y. Ai, Q.Z. Ma, P.Y. Lin, Carvacryl acetate, a semisynthetic monoterpenic ester obtained from essential oils, provides neuroprotection against cerebral ischemia reperfusion-induced oxidative stress injury via the Nrf2 signalling pathway, Food. Funct. 11 (2020) 1754–1763.
[8] J. Wang, L. Huang, C. Cheng, G. Li, J. Xie, M. Shen, Q. Chen, W. Li, W. He, P. Qiu, J. Wu, Design, synthesis and biological evaluation of chalcone analogues with novel dual antioxidant mechanisms as potential anti-ischemic stroke agents, Acta. Pharm. Sin. B. 9 (2019) 335–350.
[9] L. Huang, J. Wang, L. Chen, M. Zhu, S. Wu, S. Chu, Y. Zheng, Z. Fan, J. Zhang, W. Li, D. Chen, X. Yang, S. Wang, P. Qiu, J. Wu, Design, synthesis, and evaluation of NDGA analogues as potential anti-ischemic stroke agent, Eur. J. Med. Chem. 143 (2018) 1165–1173.
[10] R. Zhang, M. Xu, Y. Wang, F. Xie, G. Zhang, X. Qin, Nrf2-a promising therapeutic target for defensing against oxidative stress in stroke, Mol. Neurobiol. 54 (2017) 6006–6017.
[11] M. Enomoto, A. Endo, H. Yatsushige, K. Fushimi, Y. Otomo, Clinical effects of early edaravone use in acute ischemic stroke patients treated by endovascular reperfusion therapy, Stroke. 50 (2019) 652–658.
[12] Z. Guo, The modification of natural products for medical use, Acta Pharm. Sin. B. 7 (2017) 119–136.
[13] D. Rigano, C. Sirignano, O. Taglialatela-Scafati, The potential of natural products for targeting PPARα, Acta. Pharm. Sin. B. 7 (2017) 427–438.
[14] J. Wu, Y. Xi, L. Huang, G. Li, Q. Mao, C. Fang, T. Shan, W. Jiang, M. Zhao, W. He, J. Dong, X. Dong, P. Qiu, P. Yan, A steroid-type antioxidant targeting the Keap1/Nrf2/ARE signaling pathway from the soft coral dendronephthya gigantea, J. Nat. Prod. 81 (2018) 2567–2575.
[15] M. Ashrafizadeh, Z. Ahmadi, R. Mohammadinejad, T. Farkhondeh, S. Samarghandian, Curcumin activates the Nrf2 pathway and induces cellular protection against oxidative injury, Curr. Mol. Med. 20 (2020) 116–133.
[16] X. Lin, D. Bai, Z. Wei, Y. Zhang, Y. Huang, H. Deng, X. Huang, Curcumin attenuates oxidative stress in RAW264.7 cells by increasing the activity of antioxidant enzymes and activating the Nrf2-Keap1 pathway, PLoS One 14 (2019), e0216711.
[17] J.W. Shin, K.S. Chun, D.H. Kim, S.J. Kim, S.H. Kim, N.C. Cho, H.K. Na, Y.J. Surh, Curcumin induces stabilization of Nrf2 protein through Keap1 cysteine modification, Biochem. Pharmacol. 173 (2020), 113820.
[18] P. Mishra, B. Paital, S. Jena, S. Swain, S.S. Kumar, M.K. Yadav, G.B.N. Chainy, L. Samanta, Possible activation of NRF2 by Vitamin e/Curcumin against altered thyroid hormone induced oxidative stress via NFκB/AKT/mTOR/KEAP1 signalling in rat heart, Sci. Rep. 9 (2019) 7408.
[19] J. Xu, L. Zhou, Q. Weng, L. Xiao, Q. Li, Curcumin analogues attenuate Aβ25-35-induced oxidative stress in PC12 cells via Keap1/Nrf2/HO-1 signaling pathways, Chem-Biol. Interact. 305 (2019) 171–179.
[20] L. Slika, D. Patra, A short review on chemical properties, stability and nano-technological advances for curcumin delivery, Expert. Opin. Drug. Del. 17 (2020) 61–75.
[21] R. Jamwal, Bioavailable curcumin formulations: A review of pharmacokinetic studies in healthy volunteers, J. Integr. Med. 16 (2018) 367–374.
[22] R.I. Mahran, M.M. Hagras, D. Sun, D.E. Brenner, Bringing curcumin to the clinic in cancer prevention: a review of strategies to enhance bioavailability and efficacy, AAPS. J. 19 (2016) 54–81.
[23] J. Wu, Y. Zhang, Y. Cai, J. Wang, B. Weng, Q. Tang, X. Chen, Z. Pan, G. Liang, S. Yang, Discovery and evaluation of piperid-4-one-containing mono-carbonyl analogs of curcumin as anti-inflammatory agents, Bioorg. Med. Chem. 21 (2013) 3058–3065.
[24] L. Wang, W. Li, D. Cheng, Y. Guo, R. Wu, R. Yin, S. Li, H.C. Kuo, R. Hudlikar, H. Yang, B. Buckley, A.N. Kong, Pharmacokinetics and pharmacodynamics of three oral formulations of curcumin in rats, J. Pharmacokinet. Phar. 47 (2020) 131–144.
[25] P. Qiu, S. Zhang, Y. Zhou, M. Zhu, Y. Kang, D. Chen, J. Wang, P. Zhou, W. Li, Q. Xu, R. Jin, J. Wu, G. Liang, Synthesis and evaluation of asymmetric curcuminoid analogs as potential anticancer agents that downregulate NF-kappaB activation and enhance the sensitivity of gastric cancer cell lines to irinotecan chemotherapy, Eur. J. Med. Chem. 139 (2017) 917–925.
[26] L. Xiang, Q. Zhang, C. Chi, G. Wu, Z. Lin, J. Li, Q. Gu, G. Chen, Curcumin analog A13 alleviates oxidative stress by activating Nrf2/ARE pathway and ameliorates fibrosis in the myocardium of high-fat-diet and streptozotocin-induced diabetic rats, Diabetol. Metab. Syndr. 12 (2020) 1–8.
[27] Z. Xiao, F. Xu, X. Zhu, B. Bai, G. Liang, X. Shan, Y. Zhang, Y. Zhao, B. Zhang, Inhibition of JNK phosphorylation by curcumin analog C66 protects LPS-induced acute lung injury, Drug. Des. Dev. Ther. 13 (2019) 4161–4171.
[28] R. Jin, Y. Xia, Q. Chen, W. Li, D. Chen, H. Ye, C. Zhao, X. Du, D. Shi, J. Wu, G. Liang, Da0324, an inhibitor of nuclear factor-κB activation, demonstrates selective antitumor activity on human gastric cancer cells, Drug Des Devel Ther. 10 (2016) 979–995.
[29] J. Wang, D. Yun, J. Yao, W. Fu, F. Huang, L. Chen, T. Wei, C. Yu, H. Xu, X. Zhou, Y. Huang, J. Wu, P. Qiu, W. Li, Design, synthesis and QSAR study of novel isatin analogues inspired Michael acceptor as potential anticancer compounds, Eu.r, J. Med. Chem. 144 (2018) 493–503.
[30] L. Chen, Q. Li, B. Weng, J. Wang, Y. Zhou, D. Zhou, T. Sirirak, P. Qiu, J. Wu, Design, synthesis, anti-lung cancer activity, and chemosensitization of tumor-selective MCACs based on ROS-mediated JNK pathway activation and NF-κB pathway inhibition, Eur. J. Med. Chem. 151 (2018) 508–519.
[31] J.X. Qian, S. Chen, W. Shu, B. Zhang, X. Fang, Y. Chen, Z. Zhao, G. Liu, Liang, Design and synthesis novel di-carbonyl analogs of curcumin (DACs) act as potent anti-inflammatory agents against LPS-induced acute lung injury (ALI), Eur. J. Med. Chem. 167 (2019) 414–425.
[32] N. Hadzi-Petrushev, M. Angelovski, K. Rebok, V. Mitrokhin, A. Kamkin, M. Mladenov, Antioxidant and anti-inflammatory effects of the monocarbonyl curcumin analogs B2BRBC and C66 in monocrotaline-induced right ventricular hypertrophy, J. Biochem. Mol. Toxicol. 33 (2019), e22353.
[33] Y. Li, L.P. Zhang, F. Dai, W.J. Yan, H.B. Wang, Z.S. Tu, B. Zhou, Hexamethoxylated monocarbonyl analogues of curcumin cause G2/M cell cycle arrest in NCI-H460 cells via michael acceptor-dependent redox intervention, J. Agric. Food. Chem. 63 (2015) 7731–7742.
[34] G. Li, Y. Zheng, J. Yao, L. Hu, Q. Liu, F. Ke, W. Feng, Y. Zhao, P. Yan, W. He, H. Deng, P. Qiu, W. Li, J. Wu, Design and green synthesis of piperlongumine analogs and their antioxidant activity against cerebral ischemia-reperfusion injury, ACS. Chem. Neurosci. 10 (2019) 4545–4557.
[35] J. Wu, J. Li, Y. Cai, Y. Pan, F. Ye, Y. Zhang, Y. Zhao, S. Yang, X. Li, G. Liang, Evaluation and discovery of novel synthetic chalcone derivatives as anti-inflammatory agents, J. Med. Chem. 54 (2011) 8110–8123.
[36] K. Sakthivel, W. Notz, T. Bui, C.F. Barbas III, Amino acid catalyzed direct asymmetric aldol reactions: A bioorganic approach to catalytic asymmetric carbon−carbon bond-forming reactions, J. Am. Chem. Soc. 123 (2001) 5260–5267.
[37] M.K. Ghorai, S. Samanta, S. Das, Synthesis of 3,5-disubstituted cyclohex-2-en-1-one via a five-step domino reaction catalyzed by secondary amines: Formation of (E)-, β-unsaturated methyl ketones, Asian J. Org. Chem. 2 (2013) 1026–1030.
[38] V. Svetnik, Random forest: a classification and regression tool for compound classification and QSAR modeling, J. Chem. Info. Comput. Sci. 43 (2003) 1947–1958.
[39] N. Zilony-Hanin, M. Rosenberg, M. Richman, R. Yehuda, H. Schori, M. Motiei, S. Rahimipour, A. Groisman, E. Segal, O. Shefi, Neuroprotective Effect of Nerve Growth Factor Loaded in Porous Silicon Nanostructures in an Alzheimer's Disease Model and Potential Delivery to the Brain, Small 15 (2019), e1904203.
[40] T. Mei, A. Kim, L.B. Vong, A. Marushima, S. Puentes, Y. Matsumaru, A. Matsumura, Y. Nagasaki, Encapsulation of tissue plasminogen activator in pH-sensitive self-assembled antioxidant nanoparticles for ischemic stroke treatment - Synergistic effect of thrombolysis and antioxidant, Biomaterials 215 (2019), 119209.
[41] S. Li, D. Jiang, E.B. Ehlerding, Z.T. Rosenkrans, J.W. Engle, Y. Wang, H. Liu, D. Ni, W. Cai, Intrathecal Administration of Nanoclusters for Protecting Neurons against Oxidative Stress in Cerebral Ischemia/Reperfusion Injury, ACS Nano. 13 (2019) 13382–13389.
[42] P. Poprac, K. Jomova, M. Simunkova, V. Kollar, C.J. Rhodes, M. Valko, Targeting Free Radicals in Oxidative Stress-Related Human Diseases, Trends Pharmacol. Sci. 38 (2017) 592–607.
[43] G. Li, J. Gong, H. Lei, J. Liu, X.Z. Xu, Promotion of behavior and neuronal function by reactive oxygen species in C. elegans, Nat. Commun. 7 (2016) 13234.
[44] E. Parada, I. Buendia, R. León, P. Negredo, A. Romero, A. Cuadrado, M.G. López, J. Egea, Neuroprotective effect of melatonin against ischemia is partially mediated by alpha-7 nicotinic receptor modulation and HO-1 overexpression, J. Pineal Res. 56 (2014) 204–212.
[45] E.Z. Longa, P.R. Weinstein, S. Carlson, R. Cummins, Reversible middle cerebral artery occlusion without craniectomy in rats, Stroke 20 (1989) 84–91.
[46] J. Albarrán-Velo, I. Lavandera, V. Gotor-Fernández, Sequential two-step stereoselective amination of allylic alcohols through the combination of laccases and amine transaminases, Chem. Bio. Chem. 21 (2020) 200–211.
[47] E. Ballerini, L. Minuti, O. Piermatti, High-pressure diels-alder cycloadditions between benzylideneacetones and 1,3-butadienes: application to the synthesis of (r,r)-(-)- and (s,s)-(+)-delta8-tetrahydrocannabino, J. Org. Chem. 75 (2012) 4251–4260.
[48] V. Bethi, R.A. Fernandes, Traceless oh-directed wacker oxidation-elimination, an alternative to wittig olefination/aldol condensation: one-pot synthesis of α, β-unsaturated and nonconjugated ketones from homoallyl alcohols, J. Org. Chem. 81 (2016) 8577–8584.
[49] G.A. Hampannavar, R.V. Karpoormath, M.B. Palkar, M.S. Shaikh, B. Chandrasekaran, Dehydrozingerone inspired styryl hydrazine thiazole hybrids as promising class of antimycobacterial agents, ACS. Med. Chem. Lett. 7 (2016) 686–691.
[50] R. Romagnoli, P.G. Baraldi, O. Cruz-Lopez, M.K. Salvador, R. Gambari, Design, synthesis and biological evaluation of hybrid molecules containing conjugated styryl ketone and α-bromoacryloyl moieties, Lett. Drug. Des. Discov. 9 (2012) 140–152.
[51] B.P. Joshi, N.P. Singh, A. Sharma, A.K. Sinha, Microwave-assisted minutes synthesis of bioactive phenylbutanoids occurring in zingiber cassumunar, Chem. Nat. Compd. 41 (2005) 370–373.
[52] H. Yamakoshi, H. Ohori, C. Kudo, A. Sato, Y. Iwabuchi, Structure-activity relationship of c-5-curcuminoids and synthesis of their molecular probes thereof, Bioorg. Med. Chem. Lett. 18 (2010) 1083–1092.
[53] T. Chuprajob, C. Changtam, R. Chokchaisiri, W. Chunglok, N. Sornkaew, A. Suksamrarn, Synthesis, cytotoxicity against human oral cancer kb cells and structure-activity relationship studies of trienone analogues of curcuminoids, Bioorg. Med. Chem. Lett. 24 (2014) 2839–2844.

[54] L. Wenskowsky, M. Wagner, J. Reusch, H. Schreuder, H. Matter, T. Opatz, Resolving binding events on the multifunctional human serum albumin, Chem. Med. Chem. 15 (2020) 738–743.
[55] P. Joubert, D. Beaupère, A. Wadouachi, S. Chateau, B.S. Sangwan-Norreel, Effect of phenolic glycosides on agrobacterium tumefaciens virh gene induction and plant transformation, J. Nat. Prod. 67 (2004) 348–351.
[56] T. Thiemann, Solventless Wittig olefination with fluorinated benzaldehydes, J. Chem. Res. 38 (2007) 336–341.
[57] G. Rulli, K. Fredriksen, N. Duangdee, T. Bonge-Hansen, A. Berkessel, Asymmetric organocatalytic aldol reaction in water: mechanistic insights and development of a semi-continuously operating process, Cheminform. 45 (2013) 2512–2519.
[58] Y. Unoh, K. Hirano, T. Satoh, M. Miura, Palladium-catalyzed decarboxylative arylation of benzoylacrylic acids toward the synthesis of chalcones, J. Org. Chem. 78 (2013) 5096–5102.
[59] V.R. Babu Syamala, T.M. Khopade, P.K. Warghude, R.G. Bhat, An access to α, β-unsaturated ketones via dual cooperative catalysis, Tetrahedron Lett. 60 (2019) 88–91.